A PHYSICAL MODEL OF THE TROMBONE USING DYNAMIC GRIDS FOR FINITE DIFFERENCE SCHEMES

Silvin Willemsen
Multisensory Experience Lab
Aalborg University Copenhagen
Copenhagen, Denmark
sil@create.aau.dk

Stefan Bilbao, Michele Ducceschi
Acoustics and Audio Group
University of Edinburgh
Edinburgh, UK

Stefania Serafin
Multisensory Experience Lab
Aalborg University Copenhagen
Copenhagen, Denmark

ABSTRACT

We propose a complete simulation of a trombone based on finite difference schemes (FDSs). In particular, we propose a novel method to dynamically vary the grid spacing in the grid, to simulate the fact that that physical dimension of the trombone's resonator vary dynamically over time. We describe the different elements of the model and present the results of our simulations.

1. INTRODUCTION

The trombone is a musical instrument which is interesting from the simulation perspective from different viewpoints. From the point of view of the excitation, the interaction between the lips and the player has been extensively studied, and simulated mostly using a simple mass-spring damper system [1]. The sound propagation in the trombone also presents some very interesting nonlinearities, which have been investigated and simulated [2, 3, 1]. One of the interesting characteristics of this instrument is the fact that the physical dimensions of the resonator vary while playing it. Some synthesis techniques such as digital waveguides

allow to approach the issue of dynamic resonator changes in a simple and computationally efficient way, and this feature has been extensively used in real-time sound synthesis [4].

However, when modelling the resonator of the instrument using finite difference schemes (FDSs), the issue is not as trivial, and changes might compromise stability. Previous implementations of brass instruments using FDSs focus on the trumpet [5]. To our knowledge, the simulation of a trombone with varying in realtime the shape of the resonator using FDSs has not been addressed yet. We can cope with this limitation by having a grid that dynamically changes as shown in a companion paper [6].

Briefly described, we modify the grid configurations of the FDSs by adding and subtracting grid points based on parameters describing the system. In this paper we propose a full simulation of a trombone, describing in details all its elements and with a specific focus on the dynamic grid simulation.

2. CONTINUOUS SYSTEM

Wave propagation in an acoustic tube can be approximated using a 1-dimensional model. Consider a tube of time-varying length $L = L(t)$ (in m) defined over spatial domain $x \in [0, L]$ and time $t \geq 0$. Using operators ∂_t and ∂_x denoting a first-order derivative with respect to time t and space x, respectively, a system of first-order PDEs describing the wave propagation in an acoustic tube can then be written as

$$\frac{S}{\rho_0 c^2}\partial_t p = -\partial_x(Sv) \tag{1a}$$

$$\rho_0 \partial_t v = -\partial_x p \tag{1b}$$

with pressure $p = p(x,t)$ (in N/m^2), particle velocity $v = v(x,t)$ (in m/s) and (circular) cross-sectional area $S(x)$ (in m^2). Furthermore, ρ_0 is the density of air (in kg/m^3) and c is the speed of sound in air (in m/s).

Boundary conditions can then be imposed at the ends of domain, $x = 0, L$. We assume the left boundary (at the mouthpiece) to be closed and the right (at the bell) to be open according to

$$S(0,t)v(0,t) = 0, \quad \text{(Neumann, closed)} \tag{2a}$$

$$p(L,t) = 0. \quad \text{(Dirichlet, open)} \tag{2b}$$

In the following, these (lossless) boundary conditions will be modified to be coupled to a lip reed and radiating respectively.

2.1. Coupling to a Lip Reed

To excite the system, a lip reed can be modelled as a simple mass-spring-damper system. In the following, y can be seen as the moving the upper lip where the lower lip is left static and rigid. See Figure 1 for a full schematic of the lip reed model. Using dots to indicate time-derivatives the lip reed is modelled as

$$M_\mathrm{r}\ddot{y} = -M_\mathrm{r}\omega_0^2 y - M_\mathrm{r}\sigma_\mathrm{r}\dot{y} + \psi(\dot{\psi}/\dot{\eta}) + S_\mathrm{r}\Delta p, \tag{3}$$

with displacement from the equilibrium $y = y(t)$, lip mass M_r (in kg), externally supplied (angular) frequency of oscillation $w_0 = w_0(t) = \sqrt{K/M_\mathrm{r}}$ (in rad/s) and stiffness $K = K(t)$ (in N/m).

We then introduce a nonlinear collision between the lips using potential

$$\psi = \left(\frac{2K_\mathrm{c}}{\alpha_\mathrm{c}+1}[-\eta]_+^{\alpha_\mathrm{c}+1}\right)^{1/2} \tag{4}$$

$$K_\mathrm{c} > 0, \quad \alpha_\mathrm{c} \geq 1, \quad \eta \triangleq y + H_0$$

with collision stiffness K_c (in N/m if $\alpha_\mathrm{c} = 1$) dimensionless nonlinear collision coefficient α_c, distance between the lips $\eta = \eta(t)$ (in m), $[\eta]_+ = 0.5(\eta + |\eta|)$ describing the "positive part of η", and static equilibrium separation H_0 (in m).

Finally, S_r (in m^2) is the effective surface area and

$$\Delta p = P_\mathrm{m} - p(0,t) \tag{5}$$

is the difference between the pressure in the mouth P_m and the pressure in the mouth piece $p(0,t)$ (all in Pa). This pressure difference causes a volume flow velocity following the Bernoulli equation

$$U_\mathrm{B} = w_\mathrm{r}[\eta]_+ \mathrm{sgn}(\Delta p)\sqrt{\frac{2|\Delta p|}{\rho_0}}, \tag{6}$$

(in m/s) with effective lip-reed width w_r (m). Notice that when $\eta \leq 0$, the lips are closed and the volume velocity U_B is 0. Another volume flow is generated by the lip reed itself according to

$$U_\mathrm{r} = S_\mathrm{r}\frac{dy}{dt} \tag{7}$$

(in m/s). Assuming that the volume flow velocity is conserved, the total air volume entering the system is defined as

$$S(0)v(0,t) = U_\mathrm{B}(t) + U_\mathrm{r}(t). \tag{8}$$

The lip reed can then be coupled to the tube by modifying boundary condition (2a) to (8).

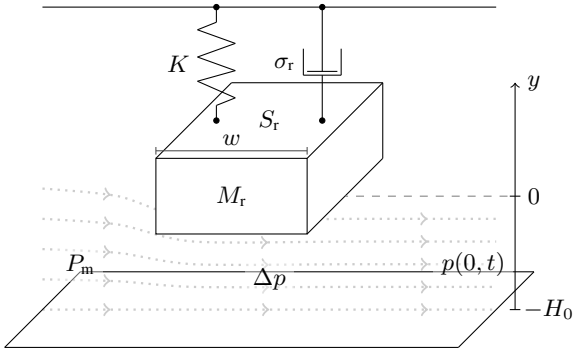

Figure 1: Lipsystem with the equilibrium at 0 and the distance from the lower lip H_0.

2.2. Radiation

As the bell-end of brass instruments is in a way “coupled" to the air, the tube loses energy at the bell, or right boundary. These losses can be modelled using a radiation model and lossless condition (2b) can be modified to be radiating instead. The radiation model used is the one for the unflanged cylindrical pipe proposed by Levine and Schwinger in [7] and discretised by Silva *et al.* in [8]. As this model is not important for the contribution of this work it will not be detailed here in full. The interested reader is instead referred to [9] for a comprehensive explanation.

3. DISCRETISATION

The continuous system described in the previous section is discretised using FDTD methods, which subdivide continuous equations into discrete points in space and time. Before moving on to this discretisation, we briefly introduce these methods along with several finite-difference operators.

3.1. Numerical Methods

Consider a 1D system described by state variable $u = u(x,t)$ with spatial domain $x \in \mathbb{R}$ and time $t \geq 0$. The spatial domain can be disctretised according to $x = lh$ with spatial index $l \in \mathbb{Z}$ and grid spacing h (in m) and time as $t = nk$ with temporal index $n \in \mathbb{Z}^{0+}$ and time step k (in s). Using these discrete variables state variable $u(x,t)$ can be discretised to grid function u_l^n.

Shift operators can then be applied to grid function u_l^n. Temporal and spatial shift operators are

$$\begin{aligned} e_{t+}u_l^n &= u_l^{n+1}, \quad e_{t-}u_l^n = u_l^{n-1}, \\ e_{x+}u_l^n &= u_{l+1}^n, \quad e_{x-}u_l^n = u_{l-1}^n, \end{aligned} \tag{9}$$

from which more complex operators can be derived. First-order derivatives can be approximated using forward, backward and centered difference operators in time

$$\delta_{t+} = \frac{e_{t+}-1}{k},\ \delta_{t-} = \frac{1-e_{t-}}{k},\ \delta_{t\cdot} = \frac{e_{t+}-e_{t-}}{2k}, \tag{10}$$

(all approximating ∂_t) and space

$$\delta_{x+} = \frac{e_{x+}-1}{h},\ \delta_{x-} = \frac{1-e_{x-}}{h},\ \delta_{x\cdot} = \frac{e_{x+}-e_{x-}}{2h}, \tag{11}$$

(all approximating ∂_x) where the identity operator 1 does not introduce any shift.

Furthermore, forward, backward and centered averaging operators can be defined in time

$$\mu_{t+} = \frac{e_{t+}+1}{2},\ \mu_{t-} = \frac{1+e_{t-}}{2},\ \mu_{t\cdot} = \frac{e_{t+}+e_{t-}}{2}, \tag{12}$$

and space

$$\mu_{x+} = \frac{e_{x+}+1}{2},\ \mu_{x-} = \frac{1+e_{x-}}{2},\ \mu_{x\cdot} = \frac{e_{x+}+e_{x-}}{2}. \tag{13}$$

Here, forward and backward averaging operators are extremely useful in the context of first-order systems as used in this paper. When applied to a grid function, the result may be interpreted as its value shifted by half a temporal or spatial step:

$$\mu_{t+}u_l^n = u_l^{n+1/2}, \quad \mu_{t-}u_l^n = u_l^{n-1/2}, \tag{14}$$

$$\mu_{x+}u_l^n = u_{l+1/2}^n, \quad \mu_{x-}u_l^n = u_{l-1/2}^n, \tag{15}$$

effectively placing the grid function on an *interleaved grid* which will be further elaborated on in the following.

3.2. Discrete Tube

We start discretising system (1) by placing velocity v on an interleaved grid, following [9], both in space and time. Domain $x \in [0, L]$ can be discretised to $l = [0, \ldots, N]$ where number of intervals between grid points is calculated using

$$N = \lfloor L/h \rfloor. \tag{16}$$

The grid functions $p_l^n \approx p(x,t)$ and $v_{l+1/2}^{n+1/2} \approx v(x,t)$ (with reduced domain $l = [0, \ldots, N-1]$) with $N+1$ and N grid points respectively are then introduced along with discrete cross-sectional area $S_l \approx S(x)$ sampled at $x = lh$ to which the spatial operators defined in Section 3.1 can also be applied.

System (1) can then be discretised into the following system of FDSs

$$\frac{\bar{S}_l}{\rho_0 c^2}\delta_{t+}p_l^n = -\delta_{x-}(S_{l+1/2}v_{l+1/2}^{n+1/2}), \tag{17a}$$

$$\rho_0\delta_{t-}v_{l+1/2}^{n+1/2} = -\delta_{x+}p_l^n, \tag{17b}$$

where $S_{l+1/2} = \mu_{x+}S_l$ and $\bar{S}_l = \mu_{x-}S_{l+1/2}$ are approximations to the continuous cross-sectional area $S(x)$. The values for $\bar{S}_l$ at the boundaries, i.e., $\bar{S}_0$ and $\bar{S}_N$ are set equal to $S(0)$ and $S(L)$.

Expanding the operators, we obtain the following recursion

$$p_l^{n+1} = p_l^n - \frac{\rho_0 c\lambda}{\bar{S}_l}(S_{l+1/2}v_{l+1/2}^{n+1/2} - S_{l-1/2}v_{l-1/2}^{n+1/2}), \tag{18a}$$

$$v_{l+1/2}^{n+1/2} = v_{l+1/2}^{n-1/2} - \frac{\lambda}{\rho_0 c}(p_{l+1}^n - p_l^n), \tag{18b}$$

where $\lambda = ck/h$ is referred to as the Courant number and

$$\lambda \leq 1 \tag{19}$$

in order for the scheme to be stable.

Finally, the boundary conditions in (2) can be discretised as

$$\mu_{x-}\left(S_{1/2}v_{1/2}^{n+1/2}\right) = 0 \tag{20a}$$

$$p_N^n = 0 \tag{20b}$$

3.3. Lip reed

As the lip reed interacts with the particle velocity of the tube, it is placed on the interleaved temporal grid, but kept on the regular spatial grid, as it interacts with the boundary at $l = 0$.

Equations (3) - (8) are discretised as follows Still need to add collision here, but I'm in doubt as to whether I want to include it at all.. The effect on the system is negligible for the values I'm using and it's going to take up a lot of space to explain:

$$M_\mathrm{r}\delta_{tt}y^{n+1/2} = -M_\mathrm{r}\omega_0^2\mu_{t\cdot}y^{n+1/2} - M_\mathrm{r}\sigma_\mathrm{r}\delta_{t\cdot}y^{n+1/2} + S_\mathrm{r}\Delta p^{n+1/2} \tag{21a}$$

$$\Delta p^{n+1/2} = P_\mathrm{m} - \mu_{t+}p_0^n \tag{21b}$$

$$U_\mathrm{B}^{n+1/2} = w[\eta^{n+1/2}]_+\mathrm{sgn}(\Delta p^{n+1/2}) \cdot \sqrt{2|\Delta p^{n+1/2}|/\rho_0} \tag{21c}$$

$$U_\mathrm{r}^{n+1/2} = S_\mathrm{r}\delta_{t\cdot}y^{n+1/2} \tag{21d}$$

$$\mu_{x-}(S_{1/2}v_{1/2}^{n+1/2}) = U_\mathrm{B}^{n+1/2} + U_\mathrm{r}^{n+1/2} \tag{21e}$$

Boundary condition (20a) can be modified to Eq. (21e), effectively coupling the lip reed to the tube.

4. DYNAMIC GRID

Arguably the most characteristic feature of the trombone is its slide with which the length of the tube is altered and the resonating frequencies are changed. In a companion article [6], we present a method to dynamically change grid configurations of FDSs by adding and subtracting grid points based on paramters describing the system. Though the paper shows changes in the wavespeed c rather than the length L, the effect of a change in either of these parameters has an identical effect on these systems as long as the geometry is unchanged for the grid points. This also means that grid spacing h does not change during the simulation, but rather the spatial domain of the system.

We can split a tube with length L into two smaller sections with lengths L_p and L_q (in m) such that $L = L_p + L_q$. Splitting the FDSs in (17) in this way yields two sets of first-order systems. The pressure and particle velocity of the first (left) system $p_{l_p}^n$ and $v_{l_p+1/2}^{n+1/2}$ are defined over discrete domains $l_p = [0, \ldots, M]$ and $l_p = [0, \ldots, M-1]$ respectively. Here, $M = \lceil L_p/h \rceil$ where $\lceil\cdot\rceil$ denotes the ceiling operation. The pressure and particle velocity of the second (right) system $q_{l_q}^n$ and $w_{l_q+1/2}^{n+1/2}$ are defined over discrete domains $l_q = [0, \ldots, M_q]$ and $l_q = [0, \ldots, M_q - 1]$ respectively. Here $M_q = \lfloor L_q/h \rfloor$ where $\lfloor\cdot\rfloor$ denotes the flooring operation. The resulting system of FDSs then becomes

$$\frac{\bar{S}_l}{\rho_0 c^2}\delta_{t+}p_{l_p}^n = -\delta_{x-}(S_{l+1/2}v_{l_p+1/2}^{n+1/2}), \tag{22a}$$

$$\rho_0\delta_{t-}v_{l_p+1/2}^{n+1/2} = -\delta_{x+}p_{l_p}^n, \tag{22b}$$

$$\frac{\bar{S}_l}{\rho_0 c^2}\delta_{t+}q_{l_q}^n = -\delta_{x-}(S_{l+1/2}w_{l_q+1/2}^{n+1/2}), \tag{22c}$$

$$\rho_0\delta_{t-}w_{l_q+1/2}^{n+1/2} = -\delta_{x+}q_{l_q}^n. \tag{22d}$$

The conditions for the outer boundaries of this system, i.e., at $l_p = 0$ and $l_q = M_q$, are the same as for the full system. The inner boundaries, $l_p = M$ and $l_q = 0$ are connected according to the method described in [6] which will be explained shortly. To calculate p_M^{n+1} and q_0^{n+1}, points outside of their respective domains seem to be needed, i.e., $v_{M+1/2}$ and $w_{-1/2}$ which in their turn need p_{M+1} and q_{-1}. In [6] we propose to calculate these *virtual grid points* based on known values of the system. Despite the fact that [6] presents the method using a second-order system, it can still be applied here. The process of how the inner boundaries are calculated is visualised in in Figure 2.

4.1. Changing the Tube Length

In the following, the location of a grid point u_l along the grid (in m from the left boundary) from is denoted as x_{u_l}.

The two pairs of first order systems in (22) are placed on the same domain x with

$$x_{p_{l_p}} = l_p h, \quad \text{and} \quad x_{q_{l_q}} = L - (M_q - l_q)h \tag{23}$$

describing the locations of the left system and right system respectively. It can be observed from Eq. (23) that as the tube length L changes, the locations of the grid points of the right system will change. More specifically, as the trombone-slide is extended and L increases, all grid points of the right system move to the right, and vice versa for a contracting slide. If L is changed in a smooth fashion, the continuous domain $x \in [0, L]$ will not necessarily be subdivided into an integer amount of intervals N (of size h). This is where a *fractional* number of intervals is introduced and is defined as

$$\mathcal{N} = L/h, \tag{24}$$

which is essentially Eq. (16) without the flooring operation, yielding $N = \lfloor \mathcal{N} \rfloor$. The fractional part of $\mathcal{N}$ can then be calculated using

$$\alpha = \alpha^n = \mathcal{N}^n - N^n, \tag{25}$$

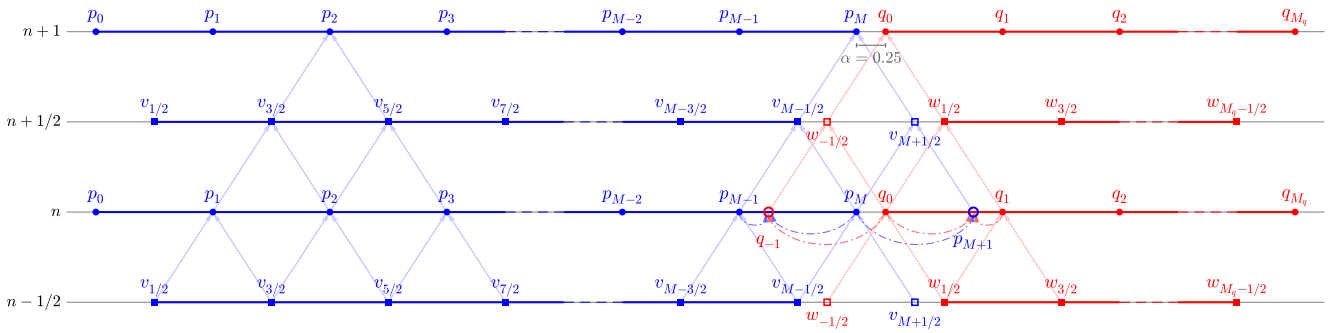

Figure 2: Schematic showing data flow of how different grid points at time index $n+1$ are calculated with $\alpha = 0.25$ in Eq. (25). To prevent cluttering, arrows going straight up (indicating that the state of a grid point at time step n is needed to calculate the state of that grid point at $n+1$) are suppressed. As an example of the usual case, the points required to calculate p_2^{n+1} are shown (refer to Eq. (18)). Furthermore, the points needed to calculate p_M^{n+1} and q_0^{n+1} are shown. The most important difference with the usual case is that the virtual grid points $p_{M_p+1}^n$ and $w_{-1/2}^n$ are the result of the interpolation of known pressure values at n using Eq. (27). .

which essentially describes the distance between the inner boundaries along the grid in terms of how many times h would fit in-between. If $\mathcal{N}^n = N^n$ and $\alpha = 0$, the inner boundaries p_M and q_0 perfectly overlap. This also means that the domain x can be exactly divided into N equal intervals of size h. As the virtual grid points p_{M+1}^n and q_{-1}^n perfectly overlap with q_1^n and p_{M-1}^n respectively, these values can be used directly to calculate the inner boundaries. This situation effectively acts as a rigid connection between the inner boundaries defined as

$$p_M^n = q_0^n. \tag{26}$$

If $\alpha \neq 0$, some other definition for p_{M+1}^n and q_{-1}^n needs to be found. We use quadratic Lagrangian interpolation according to

$$p_{M+1}^n = \frac{\alpha-1}{\alpha+1} p_M^n + q_0^n - \frac{\alpha-1}{\alpha+1} q_1^n \tag{27a}$$

$$q_{-1}^n = -\frac{\alpha-1}{\alpha+1} p_{M-1}^n + p_M^n + \frac{\alpha-1}{\alpha+1} q_0^n. \tag{27b}$$

which can then be used to calculate $v_{M+1/2}^{n+1/2}$ and $w_{-1/2}^{n+1/2}$ and consequently p_M^{n+1} and q_0^{n+1}. This process repeats every sample. It can be shown through the rigid connection in (26), that if $\alpha = 0$, the definitions in (27) reduce to $p_{M+1}^n = q_1^n$ and $q_{-1}^n = p_{M-1}^n$ as stated before.

One can change the

4.2. Adding and removing grid points

As L changes, L_p and L_q change equally $L_{\text{diff}} = L^n - L^{n-1}$, $L_p^n = L_p^{n-1} + 0.5L_{\text{diff}}$, $L_q^n = L_q^{n-1} + 0.5L_{\text{diff}}$

As the geometry varies it matters a lot where points are added and removed.

Experiments with adding / removing grid points where the geometry varies have been left for future work

5. IMPLEMENTATION

5.1. Parameters

A schematic showing the trombone geometry is shown in Figure 3 and the lengths and radii used in Table 1.

Part of tube	Length (cm)	Radius (cm)
Inner slide (1)	70.8	0.69
Outer slide (extended) (2)	53	0.72
Slide crook (3)	17.7	0.74
Outer slide (extended) (4)	53	0.72
Inner slide (5)	71.1	0.69
Gooseneck (6)	24.1	0.71
Tuning slide (7)	25.4	0.75, 1.07
Bell flare (8)	56.7 ←check	1, 10.8

Table 1: Geometry of a measured trombone taken from [10]. Numbers correspond to Figure 3.

Other parameters used in the simulation can be found in Table 2.

5.2. Order of Calculation

6. RESULTS AND DISCUSSION

The main difference with [6], is that the method is applied to a system of first-order equations rather than the second-order 1D wave equation.

The right side of the velocity "drifts"

Use average to prevent drift when $\alpha = 0$ and stays 0.

Experiments have been done with alternating between calculating the virtual grid points using the pressure and the velocity.

Rather than adding points to the left and right system in alternating fashion, points are added to pressures p and q and velocities v and w respectively

7. CONCLUSION AND FUTURE WORK

Investigate the possibility of adding / removing grid points at points where the cross-sectional area is varying.

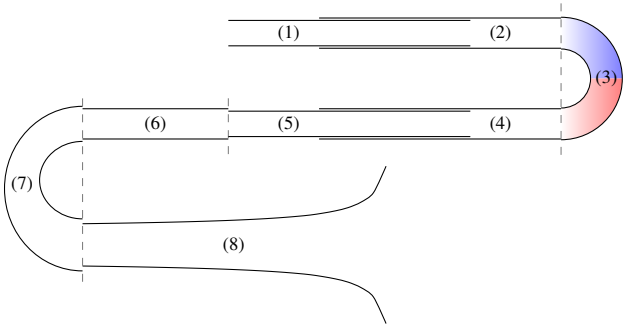

Figure 3: Schematic of the trombone. Numbers correspond to the parts of the tube found in Table 1 and dashed lines highlight where parts are separated. The scheme is split in the middle of the slide crook with the colours corresponding to those in 2.

Name	Symbol (unit)	Value
Tube		
Length	L (m)	$2.685 \leq L \leq 3.718^{\star}$
Air density	ρ_0 (kg/m^3)	1.1769**
Wave speed	c (m/s)	347.23**
Geometry	S (m^2)	See Table 1.
Lip reed		
Mass	M_r (kg)	$5.37 \cdot 10^{-5}$*
Frequency	ω_0 (rad/s)	$?? \leq \omega_0 \leq ??$
Mouth pressure	P_m (Pa)	$0 \leq P_\mathrm{m} \leq 6000??$
Damping	σ_r (s^{-1})	5*
Eff. surface area	S_r (m^2)	$1.46 \cdot 10^{-5}$*
Width	w_r (m)	0.01*
Equilibrium sep.	H_0 (m)	$2.9 \cdot 10^{-4}$*
Coll. stiffness	K_c (N/m)	10^4
Nonlin. coll. coeff.	α_c (-)	3

Table 2: List of parameter values used for the simulation. Taken from *[10], *[9] or **[11] with temperature $T = 26.85°C$.

8. REFERENCES

[1] Murray Campbell, "Brass instruments as we know them today," *Acta Acustica united with Acustica*, vol. 90, no. 4, pp. 600–610, 2004.

[2] Régis Msallam, Samuel Dequidt, Stéphane Tassart, and René Causse, "Physical model of the trombone including nonlinear propagation effects," in *ISMA: International Symposium of Music Acoustics*, 1997.

[3] Régis Msallam, Samuel Dequidt, Rene Causse, and Stephan Tassart, "Physical model of the trombone including nonlinear effects. application to the sound synthesis of loud tones," *Acta Acustica united with Acustica*, vol. 86, no. 4, pp. 725–736, 2000.

[4] Perry R Cook, *Real sound synthesis for interactive applications*, CRC Press, 2002.

[5] Reginald Langford Harrison, Stefan Bilbao, James Perry, and Trevor Wishart, "An environment for physical modeling of articulated brass instruments," *Computer Music Journal*, vol. 39, no. 4, pp. 80–95, 2015.

[6] S. Willemsen, S. Bilbao, M. Ducceschi, and S. Serafin, "Dynamic grids for finite-difference schemes in musical instrument simulations," submitted to *Proc. of the 23rd Int. Conf. on Digital Audio Effects (DAFx)*, 2021.

[7] H. Levine and J. Schwinger, "On the radiation of sound from an unflanged circular pipe," *Physical Review*, vol. 73, no. 2, pp. 383–406, 1948.

[8] F. Silva, P. Guillemain, J. Kergomard, B. Mallaroni, and A. Norris, "Approximation formulae for the acoustic radiation impedance of a cylindrical pipe," *Journal of Sound and Vibration*, vol. 322, pp. 255–263, 2009.

[9] R. L. Harrison-Harsley, *Physical Modelling of Brass Instruments using Finite-Difference Time-Domain Methods*, Ph.D. thesis, University of Edinburgh, 2018.

[10] T. Smyth and F. S. Scott, "Trombone synthesis by model and measurement," *EURASIP Journal on Advances in Signal Processing*, 2011.

[11] A. H. Benade, "On the propagation of sound waves in a cylindrical conduit," *Journal of the Acoustical Society of America*, vol. 44, no. 2, pp. 616–623, 1968.

[12] Tamara Smyth and Frederick S Scott, "Trombone synthesis by model and measurement," *EURASIP Journal on Advances in Signal Processing*, vol. 2011, pp. 1–13, 2011.

[13] JUCE, "JUCE," Available at https://juce.com/, accessed March 21, 2021.